ADVANCED FUNCTIONAL MATERIALS
www.afm-journal.de

www.MaterialsViews.com

Thermomagnetic Properties Improved by Self-Organized Flower-Like Phase Separation of Ferromagnetic $Co_2Dy_{0.5}Mn_{0.5}Sn$

Michael Schwall, Leslie M. Schoop, Siham Ouardi, Benjamin Balke, Claudia Felser, Peter Klaer, and Hans-Joachim Elmers*

A thermodynamically stable phase separation of $Co_2Dy_{0.5}Mn_{0.5}Sn$ into the Heusler compound Co_2MnSn and $Co_8Dy_3Sn_4$ is induced by rapid cooling from the liquid phase. The phase separation forms an ordered flower-like structure on the microscale. The increased scattering of phonons at the phase boundaries reduces the thermal conductivity and thus improves thermoelectric and spincaloric properties.

1. Introduction

Spincalorics, a field of research that has recently attracted a lot of interest, exploits pure spin currents induced by a thermal gradient.[1–5] Thus it promises the development of a new class of spintronic devices. In addition to a large Seebeck coefficient, a low thermal conductivity is an important physical property that has to be optimized in the course of development of advanced materials for spincalorics.

Heusler compounds with $C1_b$ or $L2_1$ structure have received much attention for thermoelectric and spincaloric applications.[6–12] The advantages of those compounds are their mechanical and thermal stability and the possibility of tailoring their physical properties via band-structure tuning.[13,14] This tuning can be realized by partial substitution of elements in the parent phase or by adding small amounts of elements into the existing compound.[13,15–17]

A characteristic property of the Heusler compounds is their high electrical conductivity, which leads on the one hand to a high power factor and on the other hand to a large thermal conductivity according to the Wiedemann–Franz law.[13,18] The main obstacle for the use of Heusler compounds in spincaloric applications is their high lattice thermal conductivity, which must be reduced to achieve a large figure-of-merit. Several approaches to reduce the lattice thermal conductivity have been proposed. Hohl et al. reported that mass disorder in the X-site lattice causes additional phonon scattering and thereby reduces the thermal conductivity.[19,20] Another approach is the creation of a nano- or microstructure in the sample by increasing the number of grain boundaries, for example by sintering of nanoparticles, by inducing a fine-grained phase separation by rapid quenching or by introducing nanoinclusions.[21–27] The challenge of this approach is to preserve structural stability over a wide temperature range. In many inhomogeneous compounds the grains of the polycrystalline sample tend to grow at higher temperatures and with increasing time. This grain coarsening reduces the grain boundaries and increases the thermal conductivity. We have achieved thermal stability in the phase separated ferromagnetic compound $Co_2Dy_{0.5}Mn_{0.5}Sn$ and show that the lattice conductivity is decreased by a factor of two due to the occurence of well-ordered flower-like phase separated structures on a very small length scale.

M. Schwall, L. M. Schoop,
S. Ouardi, Dr. B. Balke, Prof. C. Felser
Institut of Inorganic and Analytical Chemistry
University of Mainz
Staudingerweg 9, 55099 Mainz, Germany
E-mail: balke@uni-mainz.de
M. Schwall, L. M. Schoop,
Graduate School Material Science in Mainz
University of Mainz
Staudingerweg 9, 55099 Mainz, Germany
P. Klaer, Prof. H.-J. Elmers
Institut of Physics
University of Mainz
Staudingerweg 7, 55099 Mainz, Germany

DOI: 10.1002/adfm.201102792

2. Results

2.1. Structural Properties

In **Figure 1** the X-ray diffraction (XRD) pattern of $Co_2Dy_{0.5}Mn_{0.5}Sn$ is shown. Almost all reflections of the XRD pattern can be described by the reflections of Co_2MnSn (*225, Fm-3m*) and $Co_8Dy_3Sn_4$ (*186, $P6_3mc$*). The lattice parameter of the Co_2MnSn phase is $a = 5.950$ Å and the lattice parameters of the $Co_8Dy_3Sn_4$ phase are $a = b = 8.844$ Å and c = 7.518 Å, which fit well with the literature data.[28]

2.2. Phase Separation

Figure 2a shows the distribution of elements in the phase-separated $Co_2Dy_{0.5}Mn_{0.5}Sn$ compound, which form a sixfold

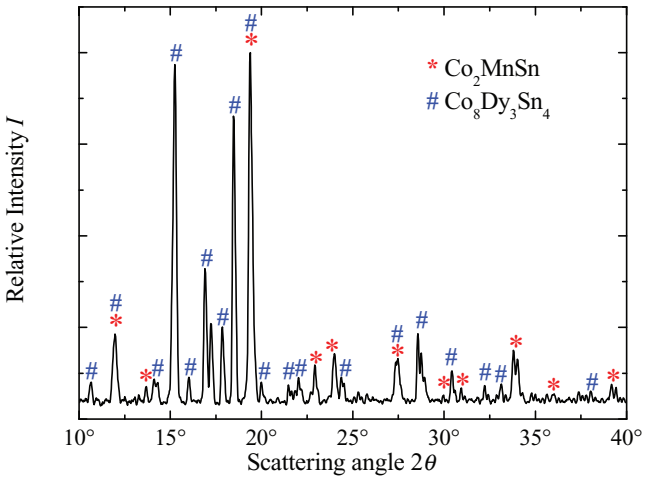

Figure 1. XRD pattern of the phase-separated $Co_2Dy_{0.5}Mn_{0.5}Sn$ alloy.

symmetry pattern. While the Co concentration is equally distributed, the Dy forms a flower-like sixfold pattern. The Dy-rich regions have a small concentration of Mn and vice versa. Sn also shows a more or less homogeneous distribution except in small regions at the grain boundaries. A linear combination of the element-specific EDX mappings shown in Figure 2b, reveals three distinct phases. Region I (light blue) shows a sixfold flower pattern embedded in region II (violet). Region III (green) fills the interstitial space inbetween region II.

The energy-dispersive X-ray (EDX) line-scan shown in Figure 2c quantifies the stoichiometry of the three regions. Region I with composition $Co_{1.95}Dy_{0.84}Mn_{0.26}Sn_{0.95}$ has the lowest Mn concentration and forms the flower-like sixfold pattern surrounded by region II with a sixfold pattern $Co_{1.95}Dy_{0.84}Mn_{0.26}Sn_{0.95}$ structure. The compositions are formally close to the Heusler alloy $Co_xDy_xMn_{1-x}Sn$. Region III consists of an intermediate composition $Co_2Dy_{0.83}Mn_{0.45}Sn_{0.72}$.

The structure in the lower left corner of Figure 2b reveals an inner pattern, roughly repeating the sixfold flower-like pattern on a smaller scale. All three phases reveal inhomogeneities that could hardly be resolved by EDX. Taking into account the XRD analysis, that has identified cubic $L2_1$ ordered Co_2MnSn and hexagonal $Co_8Dy_3Sn_4$ as pure constituent phases, the observed stoichiometry for region I and II may be interpreted in the following way: region I is dominated by the $Co_8Dy_3Sn_4$ with additional inclusions of Co_2MnSn amounting to 20% volume fraction and region II is dominated by Co_2MnSn with an amount of 10%. The scanning electron microscopy (SEM) and EDX measurements on a surface cut parallel to the temperature gradient reveals parallel stripes at up 1 mm length that can be clearly identified with regions I, region II, and region III. In contrast, EDX images on surfaces perpendicular to the temperature gradient show the flower-like structure (Figure 2). A sketch of the resulting 3D structure is shown in **Figure 3**.

The 3D cellular microstructure is formed by a dendritic crystal growth similar to observations for binary alloys, e.g., Pb-Sn.[29] The different melting points of Co_2MnSn and $Co_8Dy_3Sn_4$ are most likely the origin of the observed cellular microstructure. $Co_8Dy_3Sn_4$, with the highest melting point, solidifies as the observed region I in the remaining liquid phase. The sixfold pattern formation in region I originates from the strong epitaxial strain imposed by the hexagonal $Co_8Dy_3Sn_4$ phase with the cubic Co_2MnSn phase formed during the solidifying process.

A phase separation has also been observed for the Heusler alloys $Co_2Mn_{1-x}Ti_xSn$ and $CoTi_{1-x}Mn_xSb$.[22,30] These alloys exhibit a separation into two Heusler phases, but they show a rather irregular structure. Moreover, the phase separation disappears after high temperature annealing, in contrast to the compound discussed here.

2.3. Magnetic Properties

Figure 4a shows the magnetization as a function of the sample temperature. Two magnetic phase transitions occur at different Curie temperatures $T_{C,1} = 95 \pm 10$ K and $T_{C,2} = 830 \pm 10$ K. The T_C values were determined by fitting the temperature dependent magnetization with $M(t) = M_0(1 - T/T_C)^{1/2}$ as obtained from the mean field theory.[31] Previous measurements have shown that Co_2MnSn has a Curie temperature of $T_C = 830$ K.[9]

Therefore, the $T_{C,2}$ can be attributed to this phase. $T_{C,1}$ is likely the Curie temperature of $Co_8Dy_3Sn_4$. For pure $Co_8Dy_3Sn_4$ we found a Curie temperature of $T_C = 70 \pm 10$ K in good agreement with $T_{C,1}$. Figure 4b shows for the phase separated compound the field-dependent magnetization above and below $T_{C,1}$.

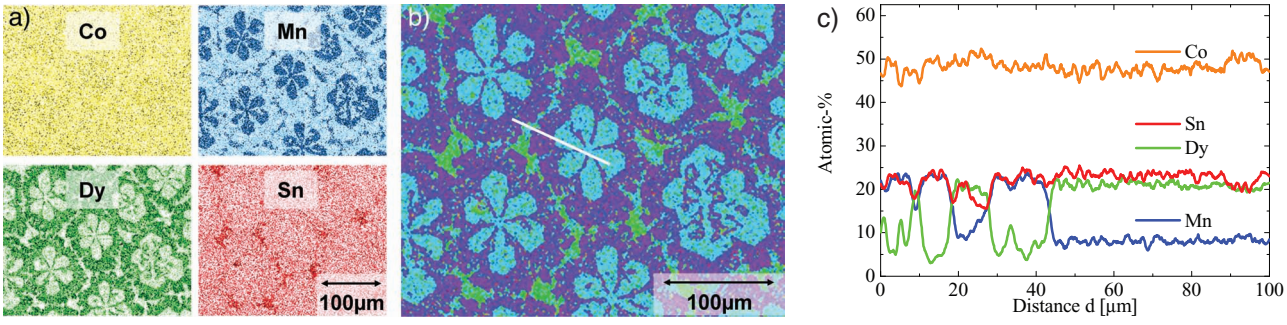

Figure 2. a) Element-specific (EDX) mappings of the four constituents of the phase separated $Co_2Dy_{0.5}Mn_{0.5}Sn$ alloy with brightness proportional to the concentration. b) Linear combina-tion of the EDX mapping shown in (a) revealing three distinct regions with different compositions: region I (light blue), region II (violet), and region III (green). c) Line-scan along the path (white line) indicated in (b).

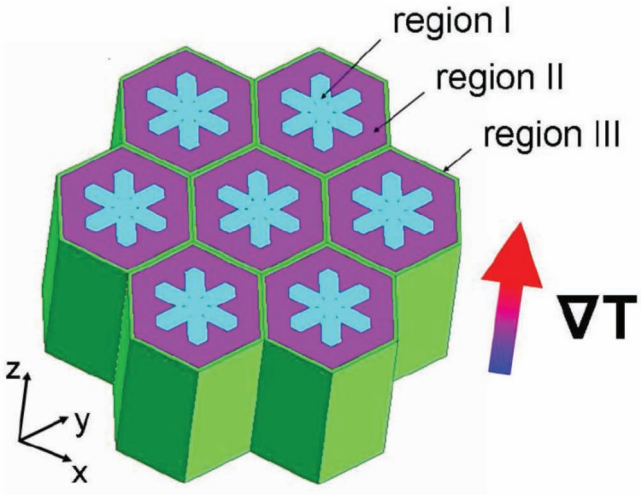

Figure 3. Sketch of the 3D phase-separated $Co_2Dy_{0.5}Mn_{0.5}Sn$ alloy. The temperature gradient ∇T is along the z direction.

At 5 K both phases are ferromagnetic, which explains the large saturation magnetization. At 300 K only Co_2MnSn exhibits ferromagnetic behavior, resulting in a much smaller magnetization. The $M(H)$ curve at 300 K reveals a coercive field of

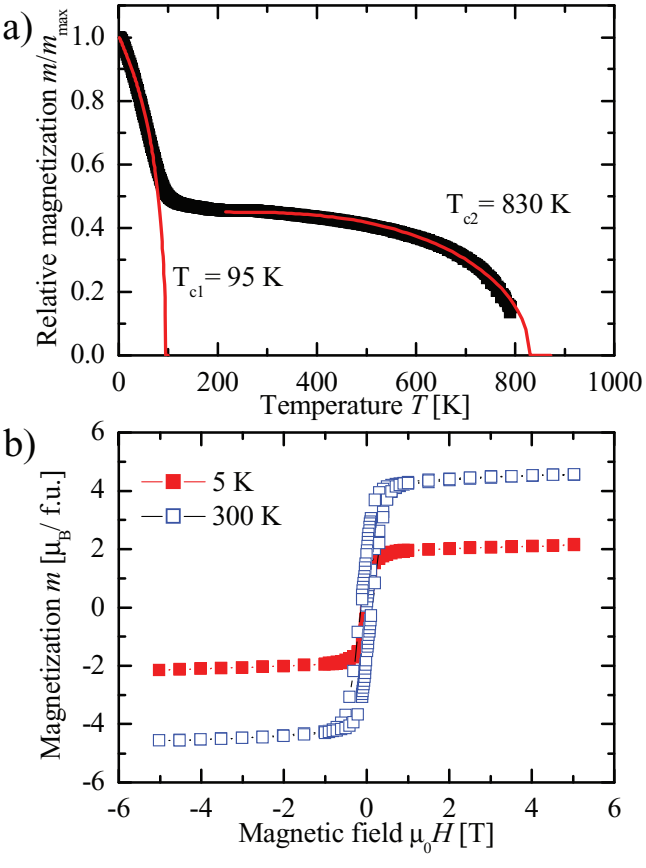

Figure 4. a) Temperature-dependent magnetization of phase separated $Co_2Dy_{0.5}Mn_{0.5}Sn$. The measurements were performed in an induction field of 1 T. b) Field-dependent magnetization at 5 K and 300 K in units of Bohr magnetons per formula unit (μB f.u.$^{-1}$).

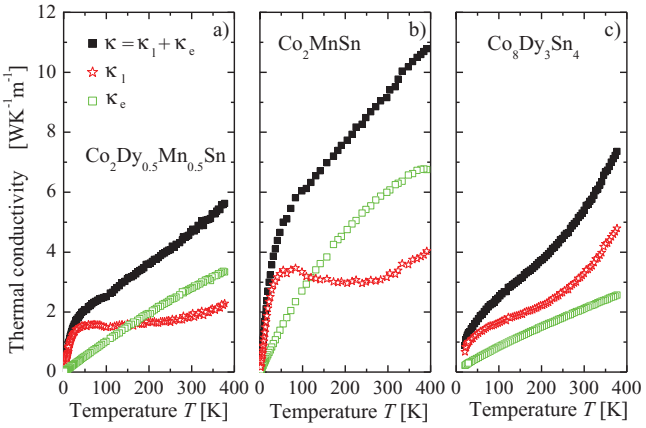

Figure 5. Temperature-dependent thermal conductivity of a) $Co_2Dy_{0.5}Mn_{0.5}Sn$, b) Co_2MnSn, and c) $Co_8Dy_3Sn_4$. Shown are the thermal conductivity, the lattice thermal conductivity and the electronic contribution to the thermal conductivity, calculated using the Wiedemann-Franz law.

$H_{c,2} = 9 \times 10^{-4}$ T. This comparatively small coercive field is on the order of magnitude observed for other Co-based Heusler alloys and indicates soft magnetic behavior.[32] At 5 K, however, the coercive field $H_{c,1} = 0.130$ T is much larger due to the crystal anisotropy of the $Co_8Dy_3Sn_4$ alloy.

2.4. Thermoelectric Properties

Figure 5 shows the thermal conductivity of the phase separated $Co_2Dy_{0.5}Mn_{0.5}Sn$ sample compared with the Heusler alloy Co_2MnSn and $Co_8Dy_3Sn_4$. The electronic contribution to the thermal conductivity κ_e was calculated using the Wiedemann-Franz Law:[18]

$$\kappa_e = L\sigma T = \frac{LT}{\rho} \quad (1)$$

where L is the Lorenz number (2.44×10^{-8} W Ω K^{-2}[33]), σ is the electric conductivity, ρ is the electric resistivity, and T is the absolute temperature. With the relation

$$\kappa = \kappa_e + \kappa_l \quad (2)$$

the lattice contribution to the thermal conductivity κ_l was calculated. In comparison to Co_2MnSn the electronic part of the thermal conductivity of $Co_2Dy_{0.5}Mn_{0.5}Sn$ is lower due to the slightly higher resistivity (**Figure 6**). The higher resistivity is probably an effect of the phase separation because there are more grain and phase boundaries than in the Co_2MnSn sample. Electrons are scattered more often at these grain boundaries. The resistivity of $Co_8Dy_3Sn_4$ is slightly higher than in the mixed compound leading to a lower electronic contribution to the thermal conductivity. The lattice thermal conductivity is about one third lower for $Co_2Dy_{0.5}Mn_{0.5}Sn$ than for Co_2MnSn. In comparison with $Co_8Dy_3Sn_4$, K_l is slightly lower than the mixed phase up to 250 K. Above 250 K the lattice thermal conductivity of $Co_8Dy_3Sn_4$ increases strongly and is about 40% higher than that of $Co_2Dy_{0.5}Mn_{0.5}Sn$.

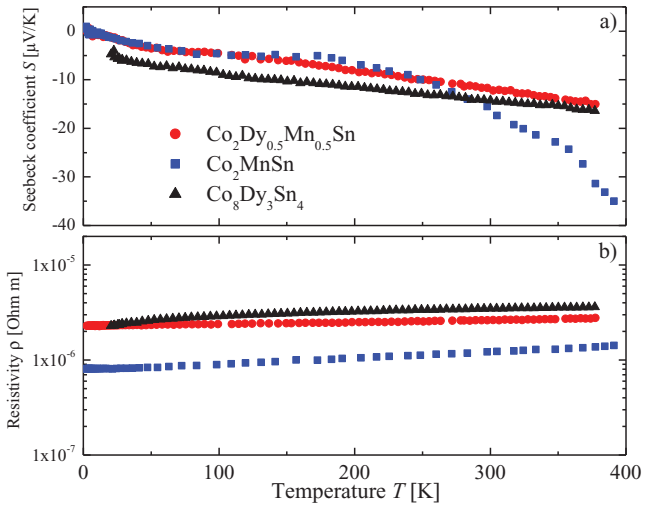

Figure 6. a) Seebeck coefficient and b) electrical resistivity for $Co_2Dy_{0.5}Mn_{0.5}Sn$, Co_2MnSn, and $Co_8Dy_3Sn_4$.

The lower κ_l value can be explained by the phase separation as well. The additional grain boundaries act as very efficient scattering centers for phonons and electrons, thus decreasing the thermal conductivity.

The lattice thermal conductivity is expected to show a maximum at intermediate temperatures due to a compensation of the increasing number of phonons contributing to the transport and increasing contribution from Umklapp processes causing scattering with increasing temperature. The additional scattering at grain boundaries cause a temperature-independent decrease of κ_l. This expected temperature dependence of $\kappa_l(T)$ is observed at lower temperatures with the maximum located at $T = 50$ K. The slight increase of the lattice thermal conductivity near 300 K can be explain by a temperature-dependent Lorenz number instead of a constant used here for the calculation of the electronic contribution to the thermal conductivity. The lattice thermal conductivity of $Co_8Dy_3Sn_4$ shows a typical behavior of a compound with a complex unit cell in a quasicrystal or amorphous metals.[34,35] $\kappa_l(T)$ can be divided into three intervals. In interval I (0–75K) the thermal conductivity increases linearly. Interval II (75–150 K) covers an almost constant $\kappa_l(T)$. In interval III ($T > 150$ K) $\kappa(T)$ increases with increasing temperature. Interval I is determined by an almost constant mean free path of the phonons, which is limited by extrinsic defects like grain boundaries, defects, or lattice distortions. In interval II, the plateau, all available phonons are saturated in the Dulong–Petit limit.[35] Interval III can be explained by the interaction of high-energy critical modes with low-energy extended phonons similar to the phonon-assisted fraction hopping in glasses.[34,35] Electrical resistivities show metallic behavior, i.e., resistivity in-creases with increasing temperature. The resistivity of $Co_2Dy_{0.5}Mn_{0.5}Sn$ is a factor of two larger. As mentioned above this is probably an effect of the phase separation. $Co_8Dy_3Sn_4$ shows a slightly higher resistivity than the mixed compound.

The Seebeck coefficient was also measured and the samples exhibit a negative Seebeck coefficient indicating n-type conduction. The Seebeck coefficient of Co_2MnSn decreases above 250 K to a value of -35 μV K^{-1} at 400 K. The Seebeck coefficient of $Co_2Dy_{0.5}Mn_{0.5}Sn$ decreases linearly with temperature in the total measured temperature range between 2 K to 400 K. Similar behavior is seen for $Co_8Dy_3Sn_4$. The electronic properties of the mixed compound $Co_2Dy_{0.5}Mn_{0.5}Sn$ seem to be dominated by the electronic properties of $Co_8Dy_3Sn_4$.

3. Conclusions

In summary, it has been shown that grain boundaries between structurally different grains can reduce the lattice thermal conductivity κ_l significantly. The lattice thermal conductivity of $Co_2Dy_{0.5}Mn_{0.5}Sn$ is lower than the mean value of the κ_l of the constituent phases. This is a consequence of the phase separation, which is temperature-stable over a wide temperature range. The temperature dependence of the magnetization reflects the phase separation into two main phases. In contrast, the magnetization curve indicates a homogeneous magnetization rotation with a large coercive field dominated by the $Co_8Dy_3Sn_4$ phase at low temperature. The Seebeck effect and the electronic resistivity in the phase separated compound are dominated by the $Co_8Dy_3Sn_4$ phase. The results of this study show that the obstacle of a large lattice thermal conductivity commonly observed for Heusler compounds can be removed by a temperature-stable phase separation. Further improvements are expected from an increase of the Seebeck coefficient by optimization of the carrier concentration through hole or electron doping.

4. Experimental Section

$Co_2Dy_{0.5}Mn_{0.5}Sn$ samples were prepared by arc melting of stoichiometric amounts of the constituents (Co 99.95%, Dy 99.9%, Mn 99.99%, Sn 99.99% from Chempur) in an argon atmosphere of 10 mbar. The samples were remelted several times to increase their homogeneity. The resulting polycrystalline ingots were annealed at 1273 K in an evacuated quartz tube for 7 days afterwards. The crystalline structure was determined by XRD using excitation by Mo $K_{\alpha 1,2}$ radiation(Bruker, AXS D8). A scanning electron microscope (Jeol JSM-6400) equipped with an EDX detection system (EUMEX EDX) was used to identify the microstucture and local stoichiometry of the phase-separated compound. The measurements were carried out at a pressure of 3×10^{-6} mbar. An acceleration voltage of 20 kV was applied and an inspection angle of 35° was set up. For the correction of the quantitative data the ZAF method was applied, which relies on atomic number (Z), absorption (A), and fluorescence (F) effects. The magnetic properties were investigated by a super-conducting quantum interference device (SQUID, Quantum Design MPMS-XL-5) using nearly punctual pieces of approximately 10 mg of the sample. The transport properties were investigated using a Physical Property Measurement System (PPMS, Quantum Design). For transport measurements the samples were cut into bars with the approximate dimensions $2 \times 2 \times 10$ mm^3. The samples were polished immediately before contacting in order to remove oxide layers. The bars were contacted with four copper leads that were wrapped around the bars to homogenize the current passing through. The sample chamber was flooded with helium and evacuated afterwards. The transport measurements were carried out at a pressure of 1.2×10^{-4} mbar by a standard four point ac method.

Acknowledgements

The authors gratefully acknowledge the financial support by the "thermoHeusler" Project (Project No. 0327876D) of the German

Federal Ministry of Economics and Technology (BMWi). M.S. and L.M.S. acknowledge the recipient of fellowships through the Excellence Initiative (DFG/GSC 266).

Received: November 18, 2011
Published online: February 22, 2012

[1] S. Hariharan, J. Gass, *Rev. Adv. Mater. Sci.* **2005**, *10*, 398.
[2] K. Uchida, S. Takahashi, H. K. J. Ieda, W. Koshibae, K. Ando, S. Maekawa, E. Saitoh, *Nature* **2008**, *455*, 778.
[3] J. Xiao, G. E. W. Bauer, K.-C. Uchida, E. Saitoh, S. Maekawa, *Phys. Rev. B* **2010**, *81*, 214418.
[4] K. Uchida, J. Xiao, J. O. Adachi, S. Takahashi, J. Ieda, T. Ota, Y. Kajiwara, H. Umezawa, H. Kawai, G. Bauer, *Nat. Mater.* **2010**, *9*, 894.
[5] C. Jaworski, J. Yang, S. Mack, D. Awschalom, J. Heremans, R. Myers, *Nat. Mater.* **2010**, *9*, 898.
[6] F. Heusler, *Verh. Dtsch. Phys. Ges.* **1903**, *5*, 219.
[7] S. Ouardi, G. H. Fecher, B. Balke, X. Kozina, G. Stryganyuk, C. Felser, S. Lowitzer, D. Kodderitzsch, H. Ebert, E. Ikenaga, *Phys. Rev. B* **2010**, *82*, 085108.
[8] J. Barth, G. H. Fecher, B. Balke, S. Ouardi, T. Graf, C. Felser, A. Shkabko, A. Weidenkaff, P. Klaer, H. J. Elmers, H. Yoshikawa, S. Ueda, K. Kobayashi, *Phys. Rev. B* **2010**, *81*, 064404.
[9] B. Balke, S. Ouardi, T. Graf, J. Barth, C. G. Blum, G. H. Fecher, A. Shkabko, A. Weidenkaff, C. Felser, *Solid State Commun.* **2010**, *150*, 529.
[10] T. Graf, J. Barth, B. Balke, S. Populoh, A. Weidenkaff, C. Felser, *Scripta Mater.* **2010**, *63*, 925.
[11] C. Felser, G. H. Fecher, B. Balke, *Angew. Chem. Int. Ed.* **2007**, *46*, 668.
[12] T. Graf, C. Felser, S. S. Parkin, *Prog. Solid State Chem.* **2011**, *39*, 1.
[13] M. Schwall, B. Balke, *Appl. Phys. Lett.* **2011**, *98*, 042106.
[14] P. Klaer, M. Kallmayer, C. G. F. Blum, T. Graf, J. Barth, B. Balke, G. H. Fecher, C. Felser, H. J. Elmers, *Phys. Rev. B* **2009**, *80*, 144405.
[15] V. Zlatić, B. Horvati, I. Milat, B. Coqblin, G. Czycholl, C. Grenzebach, *Phys. Rev. B* **2003**, *68*, 104432.
[16] S. R. Brown, E. S. Toberer, T. Ikeda, C. A. Cox, F. Gascoin, S. M. Kauzlarich, G. J. Snyder, *Chem. Mater.* **2008**, *20*, 3412.
[17] H. Li, X. Tang, X. Su, Q. Zhang, C. Uher, *J. Phys. D: Appl. Phys.* **2009**, *42*, 145409.
[18] G. Wiedemann, R. Franz, *Ann. Phys.* **1853**, *165*, 497531.
[19] H. Hohl, A. Ramirez, W. Kaefer, K. Fess, C. Thurner, C. Kloc, E. Bucher, *Mater. Res. Soc. Symp. Proc.* **1997**, *478*, 109.
[20] H. Hohl, A. Ramirez, C. Goldmann, G. Ernst, B. Wolfing, E. Bucher, *J. Phys.: Condens. Matter* **1999**, *11*, 1697.
[21] T. Graf, P. Klaer, J. Barth, B. Balke, H.-J. Elmers, C. Felser, *Scripta Mater.* **2010**, *63*, 1216.
[22] T. Graf, J. Barth, C. G. F. Blum, B. Balke, C. Felser, P. Klaer, H. J. Elmers, *Phys. Rev. B* **2010**, *82*, 104420.
[23] Y. Gelbstein, Y. Rosenberg, Y. Sadia, M. Dariel, *J. Phys. Chem. C* **2010**, *114*, 13126.
[24] M. Hatami, G. E. W. Bauer, Q. Zhang, P. J. Kelly, *Phys. Rev. B* **2009**, *79*, 174426.
[25] K. F. Hsu, S. Loo, F. Guo, W. Chen, J. S. Dyck, C. Uher, T. Hogan, E. K. Polychroniadis, M. G. Kanatzidis, *Science* **2004**, *303*, 818.
[26] J. P.A. Makongo, D. K. Misra, J. R. Salvador, N. J. Takas, G. Wang, M. R. Shabetai, A. Pant, P. Paudel, C. Uher, K. L. Stokes, P. F. P. Poudeu, *J. Solid State Chem.* **2011**, *184*, 2948.
[27] J. P. A. Makongo, D. K. Misra, X. Zhou, A. Pant, M. R. Shabetai, X. Su, C. Uher, K. L. Stokes, P. F. P. Poudeu, *J. Am. Chem. Soc.* **2011**, *133*, 18843.
[28] F. Canepa, S. Cirafici, M. Fornasini, P. Manfrinetti, F. Merlo, A. Palenzona, M. Pani, *J. Alloys Compd.* **2000**, *297*, 109.
[29] S. Tewari, R. Shah, H. Song, *Metall. Mater. Trans. A* **1994**, *25*, 1535.
[30] P. Klaer, T. Bos, M. Kallmayer, C. G. F. Blum, T. Graf, J. Barth, B. Balke, G. H. Fecher, C. Felser, H. J. Elmers, *Phys. Rev. B* **2010**, *82*, 104410.
[31] T. Graf, G. H. Fecher, J. Barth, J. Winterlik, C. Felser, *J. Phys. D: Appl. Phys.* **2009**, *42*, 084003.
[32] B. Balke, G. H. Fecher, H. C. Kandpal, C. Felser, K. Kobayashi, E. Ikenaga, J.-J. Kim, S. Ueda, *Phys. Rev. B* **2006**, *74*, 104405.
[33] A. Sommerfeld, H. Bethe, *Handbuch der Physik* vol. *24* 2nd ed., Springer Verlag, Berlin **1933**.
[34] S. Alexander, O. Entin-Wohlman, R. Orbach, *Phys. Rev. B* **1986**, *34*, 2726.
[35] C. Janot, *Phys. Rev. B* **1996**, *53*, 181.